FULL PAPER

Magnetic Resonance in Medicine 00:00–00 (2017)

Improved Dark Blood Late Gadolinium Enhancement (DB-LGE) Imaging Using an Optimized Joint Inversion Preparation and T_2 Magnetization Preparation

Tamer A. Basha,[1,2†] Maxine C. Tang,[1†] Connie Tsao,[1] Cory M. Tschabrunn,[1,3] Elad Anter,[1,3] Warren J. Manning,[1,4] and Reza Nezafat[1]*

Purpose: To develop a dark blood–late gadolinium enhancement (DB-LGE) sequence that improves scar–blood contrast and delineation of scar region.

Methods: The DB-LGE sequence uses an inversion pulse followed by T_2 magnetization preparation to suppress blood and normal myocardium. Time delays inserted after preparation pulses and T_2-magnetization-prep duration are used to adjust tissue contrast. Selection of these parameters was optimized using numerical simulations and phantom experiments. We evaluated DB-LGE in 9 swine and 42 patients (56 ± 14 years, 33 male). Improvement in scar–blood contrast and overall image quality was subjectively evaluated by two independent readers (1 = poor, 4 = excellent). The signal ratios among scar, blood, and myocardium were compared.

Results: Simulations and phantom studies demonstrated that simultaneous nulling of myocardium and blood can be achieved by selecting appropriate timing parameters. The scar–blood contrast score was significantly higher for DB-LGE ($P < 0.001$) with no significant difference in overall image quality ($P > 0.05$). Scar–blood signal ratios for DB-LGE versus LGE were 5.0 ± 2.8 versus 1.5 ± 0.5 ($P < 0.001$) for patients, and 2.2 ± 0.7 versus 1.0 ± 0.4 ($P = 0.0023$) for animals. Scar–myocardium signal ratios were 5.7 ± 2.9 versus 6.3 ± 2.6 ($P = 0.35$) for patients, and 3.7 ± 1.1 versus 4.1 ± 2.0 ($P = 0.60$) for swine.

Conclusions: The DB-LGE sequence simultaneously reduces normal myocardium and blood signal intensity, thereby enhancing scar–blood contrast while preserving scar–myocardium contrast. **Magn Reson Med 000:000–000, 2017. © 2017 International Society for Magnetic Resonance in Medicine.**

Key words: late gadolinium enhancement; myocardial scar; dark blood scar imaging

INTRODUCTION

Late gadolinium enhancement (LGE) MRI is the clinical reference standard for noninvasive imaging of left ventricle (LV) scar (1,2). Late gadolinium enhancement provides unique diagnostic and prognostic information in both ischemic and nonischemic diseases. In suspected coronary artery disease, LGE is correlated with risk of major adverse cardiac events and mortality (1,3). The peri-infarct area and scar heterogeneity on LGE imaging predict adverse outcomes in ischemic cardiomyopathy (2,4).[Kwon, 2014 #115] In hypertrophic cardiomyopathy, LGE volume predicts sudden cardiac death (5,6). In nonischemic dilated cardiomyopathy, midwall LGE predicts adverse outcomes such as sudden cardiac death (7). In mitral valve prolapse, focal LGE in papillary muscles is associated with complex ventricular arrhythmias (8).

Late gadolinium enhancement imaging uses an inversion recovery (IR) preparation pulse (9) and a Look-Locker sequence to identify the ideal inversion time (10,11). Using this approach, the normal myocardium is nulled, whereas areas of scar and blood remain bright (9). The past decades have yielded numerous advances in LGE imaging: higher spatial resolution with 3D imaging (12,13), improved detection of scar with phase-sensitive inversion recovery (PSIR) (14), free-breathing LGE (15), and faster/more efficient data acquisition (13,16). Despite these advances, low scar–blood contrast remains a major technical challenge, often making it challenging to accurately define scar–blood border (8,12). The LGE sequences also have difficulty detecting scar in thin-walled chambers, particularly the right ventricular (RV) free wall and left atrium (LA) (15,17–20).

There are several approaches to suppress the blood pool signal and improve scar–blood contrast (21–32). Multiple inversion pulse strategies decouple the blood and infarct relaxation curves (21–23). These include quadruple IR (23), double IR with slice-selective and nonselective inversions (21), and nonselective double IR with two time delays (22). However, these sequences are usually sensitive to blood flow, require precise inversion pulse timing, and penalize overall signal-to-noise ratio (SNR) and scar–myocardium contrast. The use of magnetization transfer preparation before inversion circumvents this flow dependence (24). Other methods have used motion-sensitizing gradients to create a dark blood image (25), but minimal improvement was reported in contrast studies (28). Additional images with different weighting can be acquired to improve the scar–blood contrast (29–31). The large T_2 difference between blood

[1]Department of Medicine (Cardiovascular Division), Beth Israel Deaconess Medical Center and Harvard Medical School, Boston, Massachusetts, USA.
[2]Biomedical Engineering Department, Cairo University, Giza, Egypt.
[3]Harvard-Thorndike Electrophysiology Institute, Department of Medicine (Cardiovascular Division), Beth Israel Deaconess Medical Center and Harvard Medical School, Boston, Massachusetts, USA.
[4]Department of Radiology, Beth Israel Deaconess Medical Center and Harvard Medical School, Boston, Massachusetts, USA.

Grant sponsor: NIH; Grant number: R01EB008743, R01HL129185-01, R21HL127650-01; Grant sponsor: AHA; Grant number: 15EIA22710040.

*Correspondence to: Reza Nezafat, Ph.D., Beth Israel Deaconess Medical Center, 330 Brookline Ave, Boston, MA 02215, USA. Tel: 617-667-1747; Fax: 617-975-5480; E-mail: rnezafat@bidmc.harvard.edu.

†These authors contributed equally to this work.

Received 5 October 2016; revised 8 March 2017; accepted 9 March 2017
DOI 10.1002/mrm.26692
Published online 00 Month 2017 in Wiley Online Library (wileyonlinelibrary.com).

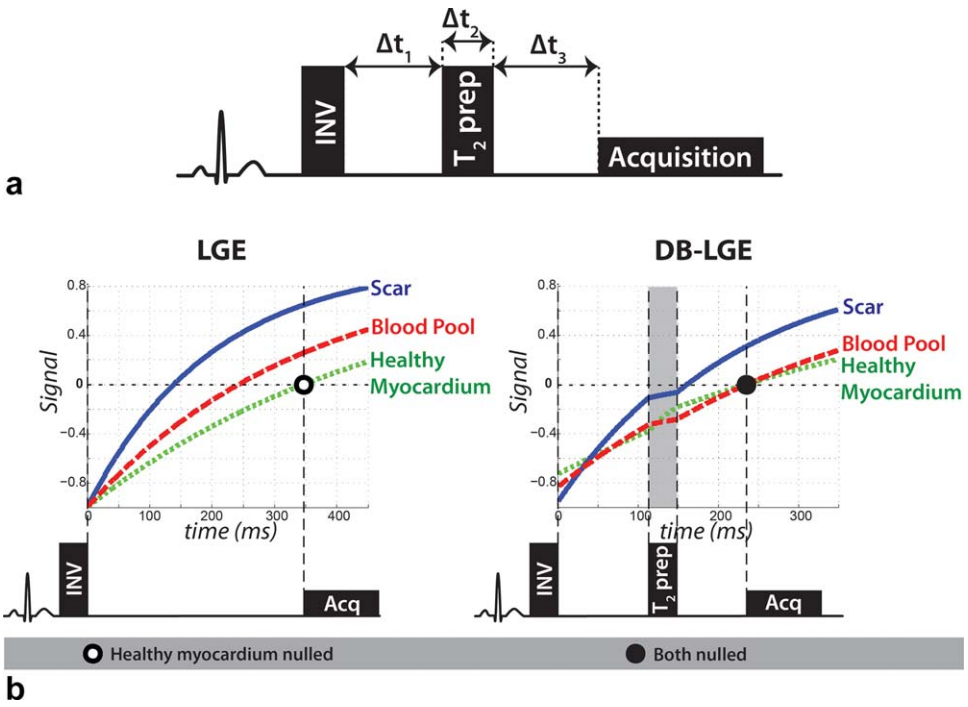

FIG. 1. (**a**) Dark blood–late gadolinium enhancement pulse sequence. After an electrocardiogram trigger, an inversion pulse (INV) is applied, followed by a pre–T_2 Prep inversion time (Δt_1) delay. A T_2 Prep pulse is then applied for an echo time of Δt_2. After the post–T_2 Prep inversion time (Δt_3) delay, the imaging signal is acquired (Acq). (**b**) The simulated signal recovery curves for the LGE sequence show that the inversion time can be chosen to null the normal myocardium (dotted green), but not the blood pool (dashed red) or scar (solid blue). The steady-state signal recovery curves for the DB-LGE sequence show that all three sequence timing parameters (Δt_1, Δt_2, and Δt_3) can be chosen to null both the blood pool and normal myocardium.

and myocardial tissue has also been exploited to improve scar–blood contrast by adding a T_2 magnetization preparation (T_2 Prep) directly before the inversion pulse (T_2 Prep IR) (32). However, in this sequence, the selection of timing parameters is challenging. Therefore, there is still an unmet clinical need to develop an LGE sequence with improved scar–blood contrast.

In this work, we propose a dark-blood LGE (DB-LGE) sequence that uses an optimized combination of IR and T_2 Prep to simultaneously null both the normal myocardium and blood pool signals by leveraging their T_2 disparity. We hypothesized that DB-LGE would increase the scar–blood contrast and improve delineation of scar region without adversely influencing the overall image quality.

METHODS

Dark-Blood LGE Pulse Sequence

A conventional LGE sequence uses an IR scheme in which T_1-weighted contrast is created to null the signal from the normal myocardium (9). In the proposed DB-LGE sequence, a T_2 Prep pulse separates the inversion pulse and image acquisition (Fig. 1a), instead of before the inversion pulse (Supporting Fig. S1). The magnetization vector (M_{RO}) produced by the DB-LGE sequence at the time of readout is

$$M_{RO} = M_0\left(1 - E_3 + E_2E_3 - \left(1 + \frac{M_{ss}}{M_0}\right)E_1E_2E_3\right), \quad [1]$$

where M_0 is the fully recovered magnetization, $E_1 = e^{-\Delta t_1/T_1}$, $E_2 = e^{-\Delta t_2/T_2}$, $E_3 = e^{-\Delta t_3/T_1}$, Δt_1 is the time between the inversion pulse and the T_2 Prep pulse, Δt_2 is the T_2 Prep pulse duration, Δt_3 is the time between the T_2 Prep pulse and the acquisition of the center line of k-space, and M_{ss} is the steady-state magnetization resulting from the short repetition times, ramp-up, and acquisition pulses that is reached after one heart beat. Derivation of the signal equation, steady-state simulations (Supporting Fig. S2), and common nulling point approximations (Supporting Fig. S3) are included in the Supporting Information.

By proper selection of Δt_1, Δt_2, and Δt_3, the blood pool and the normal myocardium can be simultaneously nulled to improve scar–blood contrast (Fig. 1b). To calculate the DB-LGE imaging parameters (Δt_1, Δt_2, and Δt_3), we developed a contrast-scout sequence to determine the common nulling point, analogous to performing a Look-Locker sequence before LGE. In the DB-LGE scout sequence, different images are acquired by fixing Δt_2 and Δt_3 and varying Δt_1 within the expected range as described subsequently.

Parameter Selection and Contrast-Scout Sequence

Numerical simulations using Bloch equations were performed to simultaneously null the blood pool and normal myocardium. Simulations were performed for different ranges of expected T_1 and T_2. The T_1 and T_2 of blood and normal myocardium were approximated from the serum gadolinium concentration using (9,33)

$$[\mathrm{Gd}]_{myo}/\rho = \lambda_{Gd} \cdot [\mathrm{Gd}]_{blood}, \quad [6]$$

$$\frac{1}{T_{1obs}} = \frac{1}{T_{1tissue}} + r_1 \cdot [\mathrm{Gd}], \quad [7]$$

where $[Gd]_{myo}$ and $[Gd]_{blood}$ are gadolinium concentration in normal myocardium and blood, respectively; ρ is the myocardial tissue density (1.05 mL/g); λ_{Gd} is the gadolinium partition coefficient (4.7 (34)); T_{1obs} is the observed T_1 of blood or myocardium with contrast;

$T_{1tissue}$ is T_1 without contrast; and r_1 is contrast agent relaxivity (7.9 L/mmol·s for Gd-BOPTA) (MultiHance, Bracco Imaging, Milan, Italy) at 1.5 Tesla (T) (35). The serum gadolinium concentration range used was 0.1 to 0.6 mmol/L (36).

Phantom Imaging

Imaging was performed on a 1.5T Philips Achieva (Philips Healthcare, Best, The Netherlands) MRI system using a 32-channel cardiac coil.

Phantom experiments were conducted to investigate the effect of DB-LGE imaging parameters (Δt_1, Δt_2, and Δt_3) on SNR and on contrast-to-noise ratio (CNR) between different vials. A commercial-grade T_1 calibration phantom (37) was used, which included nine $NiCl_2$-doped agarose vials with different T_1 and T_2 values (T_1/T_2 = 416/21, 1083/43, 454/188, 547/42, 1358/45, 1551/238, 290/41, 793/44, and 250/153 ms). Of these, three vials had similar T_1/T_2 values to postcontrast blood (454/188 ms), normal myocardium (547/42 ms), and scar (290/41 ms).

Results of the numerical simulations guided the choice of timing parameters for the contrast scout. Four different T_2 Prep durations (25, 30, 35, and 40 ms) were chosen, and simulations were conducted using the known T_1/T_2 of the vials to guide the choice of Δt_3 and the Δt_1 range for the scouts. The four scouts (each consisting of 21 single-shot DB-LGE images) were acquired with the following sequence parameters: $\Delta t_1/\Delta t_2/\Delta t_3$ = 115–215/25/110 ms, 185–285/30/85 ms, 145–245/35/70 ms, and 180–280/40/55 ms. The scout imaging parameters were as follows: field of view (FOV) = 180 × 180 mm^2, in-plane resolution = 2 × 2 mm^2, slice thickness = 8 mm, repetition time (TR)/echo time (TE) = 2.6/1.3 ms, α = 55°, acquisition window = 122 ms, and total scan time of 21 s. The DB-LGE imaging parameters were as follows: FOV = 150 × 150 mm^2, in-plane resolution = 1.5 × 1.5 mm^2, slice thickness = 8 mm, TR/TE = 5.1/2.5 ms, α = 25°, 10 linear ramp-up pulses, acquisition window = 46.7 ms. A spoiled gradient echo–based imaging sequence was used for both LGE and DB-LGE.

In Vivo Imaging

To develop and evaluate DB-LGE, we imaged 9 infarcted swine and 42 patients (56 ± 14 years, 33 male). The animal study was approved by our Institutional Animal Care and Use Committee. The protocol was approved by our institutional review board. All human subjects gave written, informed consent to participate in this HIPAA-compliant study approved by our institution's Human Subjects Committee. The LGE images were acquired 15 to 25 min after infusion of a bolus (0.1 mmol/kg in humans and 0.2 mmol/kg in animals) of gadobenate dimeglumine. All animal and human images were acquired during free-breathing and during the diastolic rest period in normal sinus rhythm. A 2D pencil beam navigator was placed on the dome of the right hemidiaphragm to compensate for respiratory motion (38). Look-Locker and DB-LGE contrast-scout sequences preceded all LGE and DB-LGE scans, respectively.

Animals

Nine Yorkshire swine (56 ± 14 kg) underwent 180-min occlusion of the left anterior descending coronary artery to create an infarct and were then allowed to recover for 36 ± 19 days before imaging (39). Three-dimensional LGE was performed before DB-LGE in all animal scans. Typical imaging parameters for free-breathing, echocardiogram-gated 3D LGE/DB-LGE were as follows: FOV = 280–320 × 280–400 × 100–120 mm^3, spatial resolution = 1–1.5 × 1–1.5 × 1–2 mm^3, TR/TE = 5.1–6.7/2.5–3.1 ms, α = 25°, sensitivity encoding rate = 2 or compressed sensing rate = 3 (13,40), 265–988 shots, scan time of 2:30–5:30 min assuming 100% navigator efficiency, centric phase-encoding order, spoiled gradient-echo-imaging readout, and single R-wave gating. No fat saturation preparation was used.

Humans

Forty-two patients referred for a clinical cardiac MRI viability assessment were recruited. Patients were referred for assessment of ischemic disease (n = 8), nonischemic cardiomyopathies (n = 28), right ventricular dysplasia (n = 1), cardiac lymphoma (n = 1), mitral valve prolapse (n = 3), and pulmonary sarcoidosis (n = 1). No patient had recent (< 6 months) history of myocardial infarction. Presence or absence of microvascular obstruction was not assessed. Patients were imaged using our standard clinical viability imaging protocol of 3D PSIR (14,31) and/or LGE and DB-LGE. Ten patients were imaged only with 3D-PSIR LGE (alternate R-wave gated), and the remainder with 3D LGE (single R-wave gated). All patients were imaged with 3D-DB LGE. The order of 3D-DB LGE and 3D-PSIR-LGE/3D-LGE acquisition was randomized. The typical imaging parameters for free-breathing, ECG-gated images were TR/TE = 5.1/2.5 ms, α = 25°, FOV = 300–400 × 300–400 × 80–120 mm^3, spatial resolution = 1.5 × 1.5 × 3–5mm^3, and sensitivity-encoding rate = 2, 141 shots, scan time of 2:30–4:00 min assuming 100% navigator efficiency, centric phase-encoding order, with spoiled gradient-echo-imaging readout. The FOV, resolution, and scan time varied among the different patients to accommodate for patient size and heart rate, but were matched for LGE and DB-LGE acquisitions.

Data Analysis

For the phantom study, signal intensities were measured from different vials by manually drawing regions of interest within each vial. The CNR was calculated for vials with T_1/T_2 values similar to scar, blood, and myocardium. For the qualitative analysis of in vivo images, two expert readers (RN with 15 years and CT with 10 years of experience in cardiac MR) independently scored all images. Readers assigned "yes/no" for diagnostic quality and for presence of LGE. Overall image quality was assessed using a 4-point scale with score 1 = poor to 4 = excellent). Overall image quality was scored based on the presence of image artifacts and the quality of suppression of the normal myocardium signal, independent of scar visualization. Similarly, scar–blood contrast was

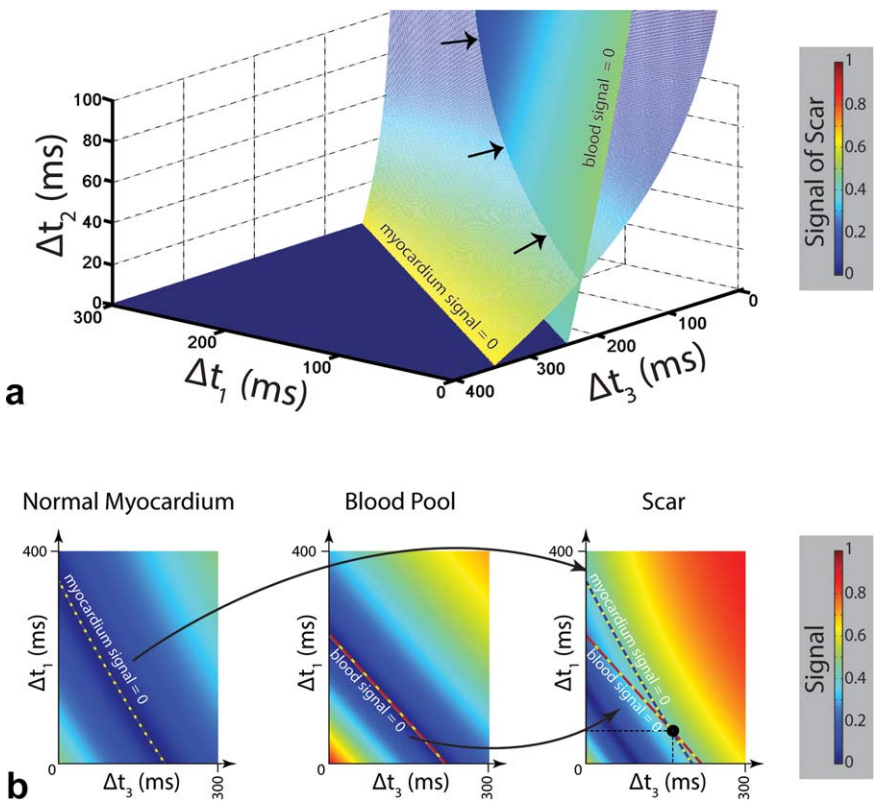

FIG. 2. (**a**) Three-dimensional representation of the zero planes of normal myocardium and blood pool signals. The line of intersection (arrows) represents the common nulling points. (**b**) Simulations of the steady-state signal intensity produced by DB-LGE as a function of Δt_1 and Δt_3 (Δt_2 = 35 ms) for normal myocardium, blood pool, and scar. The color represents the normalized signal magnitude. The zero lines of the normal myocardium (blue) and blood pool (red) signals are superimposed on the scar signal plot. The coordinates of the intersection of these zero lines (black dot) give the common nulling point.

scored from 1 = poor to 4 = excellent. Any disagreement in the presence or absence of enhancement was reviewed in a subsequent consensus reading by both readers. For scans with scar on LGE, the average signal intensities in normal myocardium, LV blood pool, and LV scar were measured from corresponding slices, in which scar was visible on both sequences. Regions of interest were manually contoured and matched between the scans. These values were used to calculate the signal ratios of scar–myocardium and scar–blood. Patients with only PSIR scans for comparison were excluded from the quantitative analysis. The qualitative scores were compared using a Wilcoxon signed-rank test for paired samples. Signal ratios were compared using a paired t-test. Analyses were performed using R Statistical Software (version 3.2.3, Foundation for Statistical Computing, Vienna, Austria). Statistical significance was defined as $P < 0.05$.

RESULTS

Numerical Simulations

Assuming a fixed T_1/T_2 for blood (T_1/T_2 = 350/250 ms), normal myocardium (T_1/T_2 = 500/50 ms), and scar (T_1/T_2 = 200/70 ms), numerical simulations of the DB-LGE sequence reveal that blood and normal myocardium signals each become zero along a unique plane. These planes intersect along a curve, representing the points at which both tissues are nulled (arrows in Fig. 2a). Along this line, a minimum T_2 Prep duration is required for nulling, but the scar signal is maximized at lower T_2 Prep durations. A simplified representation of the numerical simulations (Fig. 2b) demonstrates that the T_2 Prep time can be fixed to identify one common nulling point (ie, a $\Delta t_1/\Delta t_3$ combination that simultaneously nulls both the blood pool and normal myocardium). The results were similar for different ranges of T_1/T_2 values for each tissue (not shown).

Simulations of contrast washout guided the process of restricting Δt_2 and Δt_3 parameters to simplify the protocol. Based on these simulations, a Δt_2 of 35 ms is the lowest duration that enables blood-pool suppression for a wide range of gadolinium concentrations (Fig. 3a). When Δt_2 is fixed at 35 ms, Δt_3 of the common nulling point plateaus at approximately 150 ms over a realistic range of serum gadolinium concentrations (36), indicating that it is stable over much of the contrast washout period (Fig. 3b). Therefore, fixing Δt_2 and Δt_3 can simplify parameter selection based on contrast concentration, biodistribution, and relaxivity.

Phantom Imaging

The phantom experiment demonstrated the relationship of the DB-LGE signal to the sequence timing parameters (Fig. 4). A numerical simulation using the measured T_1 and T_2 values of the targeted vials successfully determined the common nulling points. The DB-LGE sequence was able to achieve complete nulling of the vials with similar T_1/T_2 to normal myocardium and blood pool at all four Δt_2 times. The common nulling points for the four scans had $\Delta t_1/\Delta t_2/\Delta t_3$: 210/40/55, 195/35/70, 185/30/85, and 140/25/110 ms. The scar–myocardium vial CNR measurements for these parameters were 5.3, 5.9, 6.6, and 6.8, respectively. The scar–blood CNR measurements were 4.5, 5.6, 6.8, and 7.5, respectively.

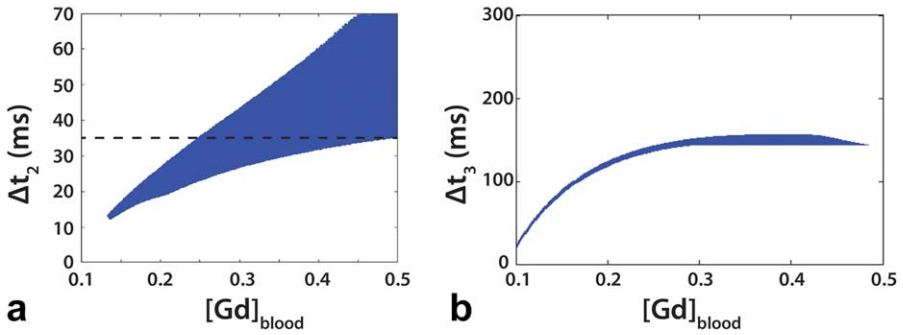

FIG. 3. Plot of Δt_2 (**a**) and Δt_3 (**b**) needed to achieve the common nulling point versus gadolinium concentration in the blood pool. Allowing for a range of Δt_1 and Δt_3, the nulling point can be achieved with a wide range of Δt_2 durations (shaded blue region). $\Delta t_2 = 35$ ms (dashed line) is the lowest T_2 Prep duration that achieves a common nulling point over the widest range of gadolinium concentrations. When Δt_2 is fixed at 35 ms, the Δt_3 of the nulling point plateaus over a wide range of gadolinium concentrations, suggesting that a scout with $\Delta t_2 = 35$ ms and $\Delta t_3 = 150$ ms sampling Δt_1 from 15 to 115 ms will be able to identify the common nulling point within a long time period after contrast administration.

The CNR, SNR, and signal ratios (scar–myo, scar–blood) for the phantom experiments are shown in Supporting Figure S4. The SNRs of the scar and blood vials are higher in LGE as compared with DB-LGE, regardless of the T_2 Prep duration. The scar vial SNR was lower in the DB-LGE scan by a factor of 0.54 to 0.75 (T_2 Prep duration 40–25 ms, respectively). The scar–myo are higher on the LGE scans than the DB-LGE, but the difference in the scar–myo CNR and scar–blood CNR is much greater than in DB-LGE. The scar–blood ratio on the LGE scan is lower than that seen on the DB-LGE scans.

Based on the results of our numerical simulations and phantom study, we designed the contrast scout sequence that was used in all subsequent in vivo studies. The

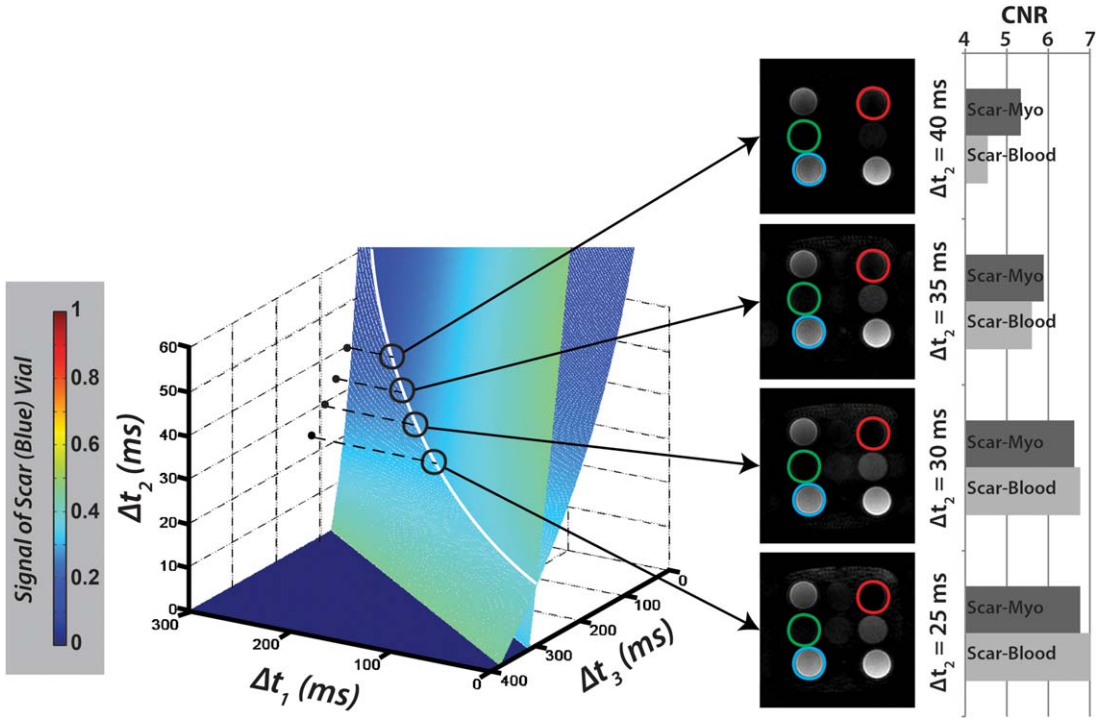

FIG. 4. Numerical simulation of parameters needed to simultaneously null two vials in the phantom based on their T_1 and T_2 values and the corresponding phantom scans with vials representing scar (blue), normal myocardium (green), and blood (red). As in Figure 3, each plane represents the parameters needed to null just one vial; the line of intersection (white line) provides the parameters of the common nulling points. The superimposed color represents the expected signal of the blue vial at each point in the parameter space. The black circles on the plot identify the four points in parameter space that were used to create the phantom scans ($\Delta t_2 = 25$, 30, 35, and 40 ms). Arrows point to phantom scans that use the DB-LGE sequence to intentionally null the green and red vials, whose T_1 and T_2 values are similar to the target tissues. The corresponding LGE scan with the normal myocardium vial (green) nulled is included. The parameters $\Delta t_1/\Delta t_2/\Delta t_3$ used to acquire the scans were 210/40/55, 195/35/70, 185/30/85, and 140/25/110 ms.

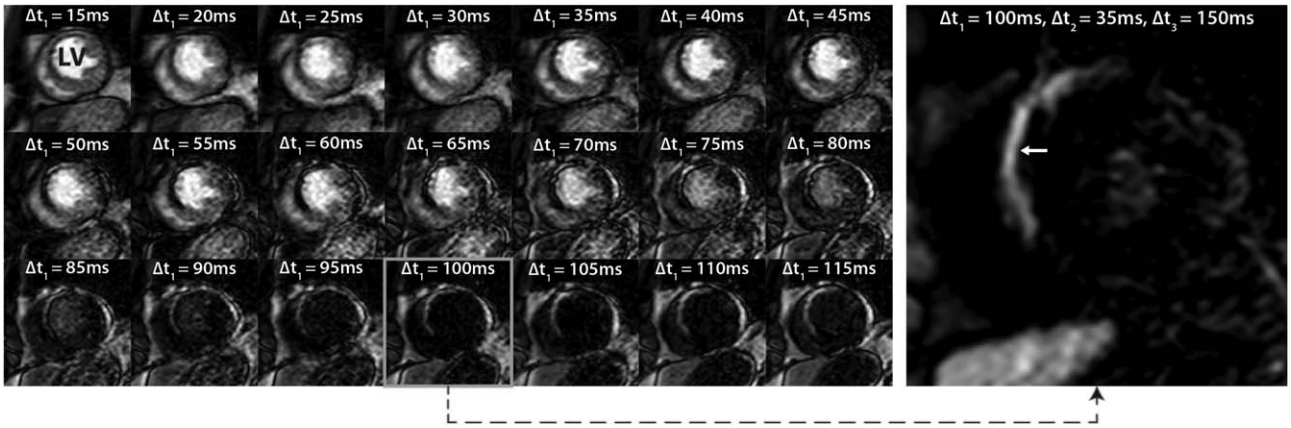

FIG. 5. Example of the contrast-scout sequence in the LV short-axis plane, and resulting DB-LGE image in a patient (61-year-old male) with a large primarily LV scar (arrow) secondary to infarction of the mid–left anterior descending coronary artery. A total of 21 low-resolution, single-slice images are acquired to finely sample a range of Δt_1 values after setting Δt_2 and Δt_3 constant. The image that best nulls both the blood and normal myocardium is visually identified, and the Δt_1 value used to create that image is applied to create the DB-LGE image (right). With one quick scouting sequence, the optimal sequence timing is identified.

scout sequence fixes $\Delta t_2/\Delta t_3$ at 35/150 ms and samples Δt_1 between 15 and 115 ms with 5-ms increments, yielding 21 images with different tissue contrast. To select the correct timing, the technologist visually identifies the image with suppressed blood pool and normal myocardium, and calculates the associated timing parameter (ie, Δt_1) value (Fig. 5). We note that because the T_1/T_2 values of vials in phantom were static, the phantom experiment did not replicate physiological gadolinium washout and required slightly different sequence parameters than the in vivo studies because of differences in T_1 and T_2.

In Vivo Imaging

The operator identified the suitable timing on the contrast-scout scan in all cases. In the swine models, the myocardium is nulled by both sequences (Fig. 6). A high dose of contrast agent (0.2 mmol/kg of Gd-BOPTA) resulted in high blood signal and reduced contrast between the blood pool and the scar in the swine studies. Although the blood pool is not completely nulled in the DB-LGE images, the scar is brighter than the blood pool, which more readily allows for robust scar–blood delineation. In patients who received 0.1 mmol/kg of Gd-BOPTA, areas of hyperenhancement reflect the poor scar–blood contrast often seen in LGE/PSIR images. In comparison, the blood pool and normal myocardium are completely nulled to improve scar–blood contrast in DB-LGE images (Figs. 7a–7d, Supporting Videos S1 and S2).

Representative line intensity profiles (Fig. 8) demonstrate the abrupt change in signal intensity at the border between scar and blood in DB-LGE images as compared with LGE. In the qualitative assessment (Table 1), reader 1 identified all scans to be diagnostic, whereas reader 2 identified 5 of 42 of LGE and 2 of 42 DB-LGE to be nondiagnostic. Those with nondiagnostic images had motion artifacts or incomplete nulling of myocardium. Hyperenhancement was present in all animals and 22 of patients on the consensus reading. Of the patients with LV scar, 18 of 22 were imaged with LGE/PSIR before DB-LGE, and 14 of 17 were imaged with LGE before DB-LGE. Discrepancies in identification of presence/absence of scar arose because isolated papillary muscle hyperenhancement was missed in two patients on the independent read. Agreement on the presence/absence of scar was reached on the consensus reading, and scoring was performed accordingly. Despite the expected loss of SNR as a result of T_2 Prep use in the DB-LGE sequence, the overall image quality scores were similar between the two sequences. The qualitative scar–blood contrast scores (Table 1) from both readers were significantly greater in DB-LGE ($P < 0.05$). In the quantitative analysis of the patients with LV scar and LGE scans available for comparison (n = 17), the scar–blood ratio was significantly higher in DB-LGE for both infarcted swine and

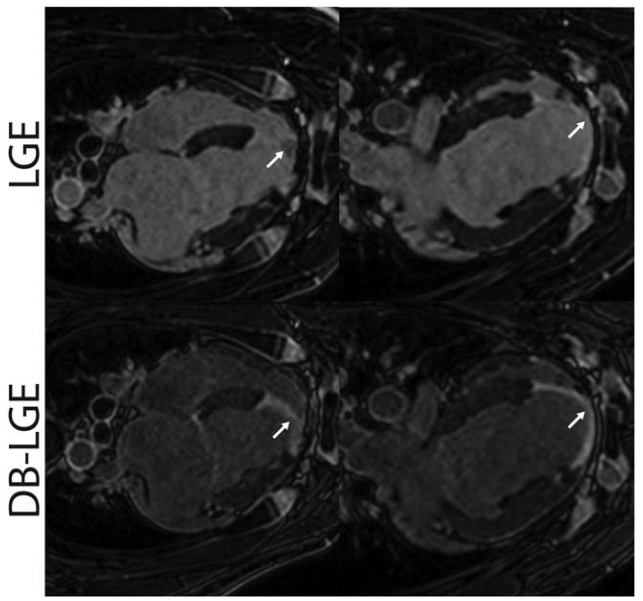

FIG. 6. Comparison of DB-LGE (bottom row) and LGE (top row) images from two swine with LV infarcts, demonstrating improvements in blood–myocardium contrast. Note that the DB-LGE sequence more readily allows for identification of the scar–blood border (arrows).

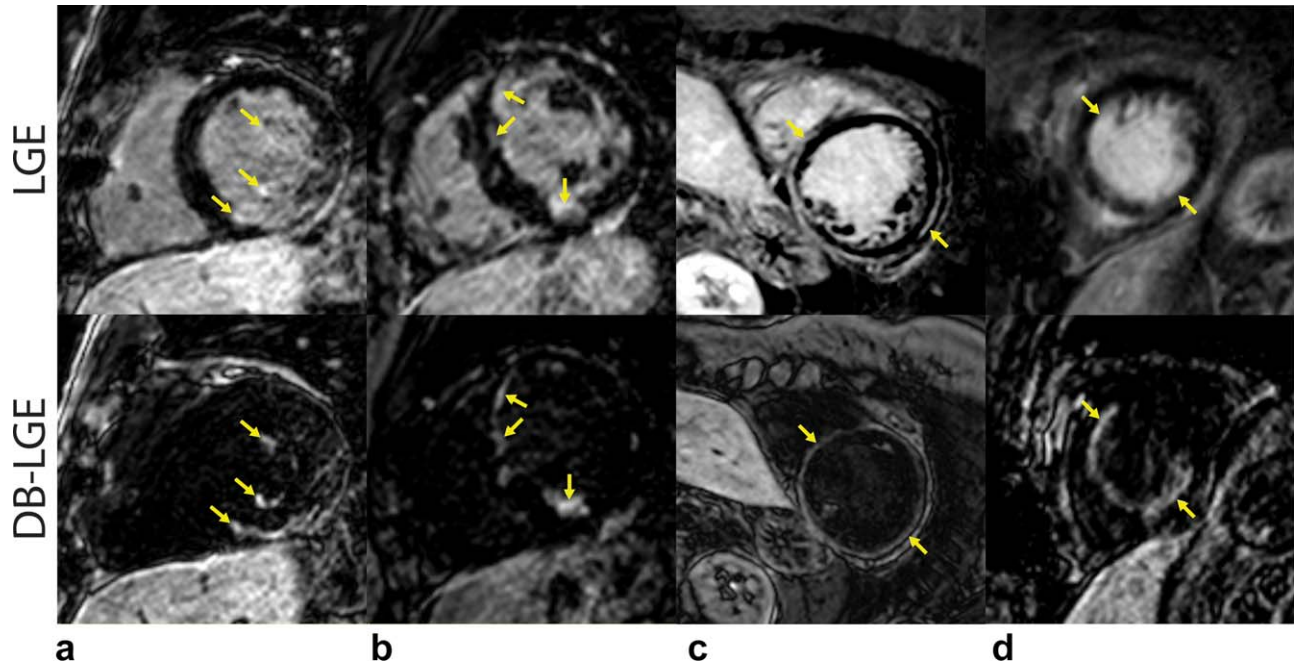

FIG. 7. Comparison of DB-LGE (bottom) to LGE/PSIR (top) images in patients with LV scar (see arrows): (**a**) 70-year-old male with history of myocardial infarction and inferior scar and papillary muscle enhancement visible on DB-LGE but not LGE; (**b**) 52-year-old female with ischemic heart disease and multiple areas of enhancement visible on both LGE and DB-LGE; (**c**) 62-year-old female with LV noncompaction and LV mid-wall enhancement visible on both PSIR and DB-LGE; (**d**) 62-year-old female with multivessel coronary artery disease. DB-LGE improves scar–blood contrast compared with PSIR.

humans ($P \leq 0.002$), but the scar–myocardium ratio was similar ($P > 0.05$) (Table 2).

DISCUSSION

The DB-LGE sequence improves visualization of myocardial scar by simultaneously suppressing the signal from both the blood pool and normal myocardium. The optimal timing parameters of the DB-LGE sequence are identified using a contrast-scout scan performed before DB-LGE, analogous to a Look-Locker sequence in conventional LGE. The contrast between the blood pool and scar can be readily adjusted by changing these timing parameters. The DB-LGE sequence does not increase the scan time and requires no postprocessing analysis, facilitating its clinical adoption.

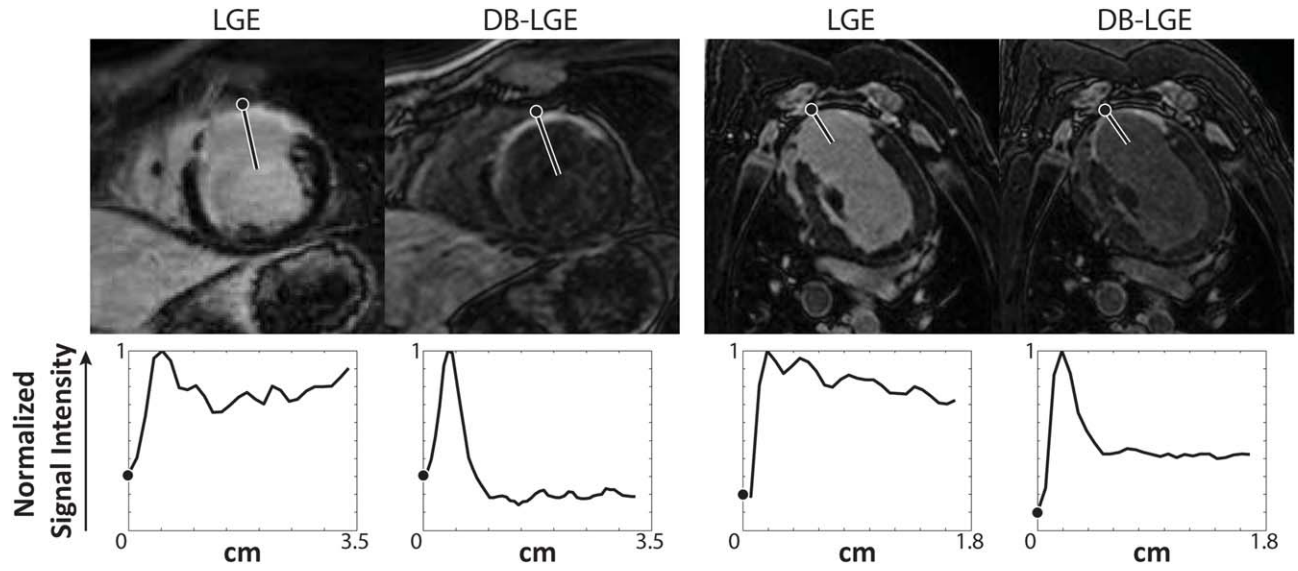

FIG. 8. Representative LGE and DB-LGE line intensity signed profiles in one patient (62-year-old male, left) and one swine (right). The interrogation line is drawn from the epicardial edge of the myocardium to the center of the LV blood pool, passing through the scar. The signal intensities, normalized to the maximum signal, along that line are plotted below the corresponding image to show the lower signal drop-off from scar to blood in LGE images compared with DB-LGE images.

Table 1
Subjective LGE Presence, Overall Image Quality, and Scar–Blood Contrast Scores of LGE and DB-LGE Images

		Diagnostic[a]		LGE present[a,b]		Overall image quality score[c]		Scar–blood contrast score[d]	
		Animal (n = 9)	Patient (n = 42)	Animal (n = 9)	Patient (n = 42)	Animal (n = 9)	Patient (n = 42)	Animal (n = 9)	Patient (n = 22)
Reader 1	LGE	9/9	42/42	9/9	22/42	3.0 ± 0.7	3.5 ± 0.6	1.9 ± 1.1	3.1 ± 0.7
	DB-LGE	9/9	42/42	9/9	22/42	3.6 ± 0.5	3.5 ± 0.6	3.0 ± 0.8	3.8 ± 0.4
	P					0.037	0.57	0.013	0.004
Reader 2	LGE	9/9	37/42	9/9	22/42	3.1 ± 0.8	3.2 ± 0.7	1.9 ± 0.3	2.5 ± 0.6
	DB-LGE	9/9	40/42	9/9	22/42	3.3 ± 0.5	3.1 ± 0.7	3.6 ± 0.5	3.4 ± 0.6
	P					0.48	0.81	0.008	< 0.001

[a]Number of scans scored as "yes" out of the total number of scans scored.
[b]Includes results of consensus reading.
[c]1 = significant artifact/poor suppression of normal myocardium; 2 = moderate artifact/limited suppression; 3 = minimal artifact/good suppression; 4 = no significant artifact/excellent suppression.
[d]1 = cannot identify scar–blood border; 2 = can confidently identify < 50% of border; 3 = can confidently identify > 50% of border; 4 = can identify entire scar–blood border.

Previous attempts to use a T_2 Prep to suppress the bright blood in LGE demonstrated the potential efficacy of this strategy, but the method was never fully optimized for the myocardium. Liu et al (32) proposed a DB-LGE sequence using a T_2 Prep-IR preparation sequence, in which a T_2 Prep is played immediately before the inversion pulse. This ordering restricts the dynamic range of the sequence, causing the ideal T_2 Prep and inversion times to change rapidly over the contrast washout period (Supporting Fig. S6). As a result, it becomes challenging to identify the optimal timing robustly (numerical simulation of the signal behaviors is included in the Supporting Information). Bangerter et al previously demonstrated an analogous T_2 Prep-IR-catalyzed steady-state free-precision sequence for noncontrast-flow independent peripheral angiography, which improves the contrast of blood against muscle and synovial fluid (41). The magnetization preparation is similar to the proposed sequence, but does not require real-time optimization of sequence timing parameters, as the regime of tissue T_1/T_2 values targeted by noncontrast angiography is significantly higher and less dynamic.

In DB-LGE, timing parameters can be adjusted to achieve different blood–myocardium contrast. The proposed contrast-scout sequence provides images with different contrasts between blood and myocardium, from which the technologist may choose the parameters that yield the desired CNR. The acquisition parameters of the contrast scout scan are different than the DB-LGE scan parameters, which might result in a slight difference in the optimal timing predicted by the contrast scout, but this error is likely outweighed by the error from the subjection nature and discretization of the scout protocol (similar to the Look-Locker scout used in LGE imaging). Alternate contrast-scout protocols could be implemented, an example of which is discussed in the Supporting Information (Supporting Fig. S5). Comparing image quality between human and swine studies, we have found the "gray blood" images in our swine provide a better definition of scar and its location. Future studies are warranted to investigate the degree of nulling that may improve interpretation of DB-LGE data.

Table 2
Objective Scar–Myocardium and Scar–Blood Signal Ratios in LGE and DB-LGE

	Scar/Myocardium		Scar/Blood	
	Animals (n = 9)	Patients (n = 17)	Animals (n = 9)	Patients (n = 17)
LGE	4.1 ± 2.0	6.3 ± 2.6	1.0 ± 0.36	1.5 ± 0.53
DB-LGE	3.7 ± 1.1	5.7 ± 2.9	2.2 ± 0.73	5.0 ± 2.8
P	0.60	0.35	0.002	< 0.001

We did not use a PSIR sequence, because all scar images were acquired using 3D imaging. A PSIR acquisition increases the scan time. However, the proposed sequence can be readily adopted for PSIR imaging as shown recently by Kellman et al (42). Arrhythmias could potentially affect blood-pool suppression as a result of increased signal variation, resulting in artifacts such as ghosting. However, all patients in our study were in sinus rhythm during the scan, and we did not study the effect of arrhythmia on DB-LGE image quality. The inversion delay (ie, time between the inversion and imaging) of DB-LGE is shorter than standard LGE. As a result, DB-LGE could potentially facilitate systolic scar imaging, which may be beneficial for patients not in sinus rhythm. As shown in the numerical simulation and phantom, the nulling point can also be determined analytically if the T_1 and T_2 of each tissue is known a priori. This can be achieved by performing T_1 and T_2 mapping sequences before the DB-LGE sequence.

Despite these benefits, there are also several technical limitations to the proposed sequence. The DB-LGE images have lower SNR compared with LGE images, as a result of of signal loss associated with T_2 Prep pulse. Despite SNR loss, increased scar–blood CNR results in improved scar detection. Further studies are warranted to investigate the optimal selection of imaging parameters by including desired SNR and CNR as additional criteria. In the DB-LGE sequence, the fat signal recovers similar to scar, resulting in similar signal intensity, and could potentially be confused with scar to create a false positive. In our current DB-LGE sequence, we did not

incorporate any fat saturation; however, fat saturation is essential for clinical adoption of DB-LGE, and further investigation into design of a robust fat saturation in DB-LGE is needed. Insufficient blood-pool suppression could also potentially result in false identification of scar.

Our study has several limitations. Patients were recruited among those referred for a clinical cardiac MR viability exam and imaged after 0.1 mmol/kg of Gd-BOPTA, the standard clinical dose/contrast agent in our medical center. The swine study was performed as part of an ongoing study of ventricular arrhythmia and ablation (43), which uses a 0.2-mmol/kg dose of Gd-BOPTA. Therefore, the contrast dose was different for animal versus human studies, which may have contributed to different level of blood suppression and image quality between the DB-LGE images in human and swine studies. Further studies to investigate the performance of DB-LGE for different contrast agent, dose, and timing after contrast injection are needed.

The phantom experiment does not take into account the inflow of fresh blood or dynamic gadolinium washout. There were differences in imaging parameters between DB-LGE and LGE/PSIR, and in some cases, only PSIR was available for comparison. We are unable to quantify in vivo SNR/CNR because of the parallel imaging or compressed-sensing reconstruction combined with the imbalanced acquisition order, despite randomization. Scar size was not used as a metric for comparison, because one cannot verify which measurement is more accurate. We did not perform any histology in our swine study, because additional scar was created during radiofrequency ablation. Our study does not demonstrate that improved scar–blood contrast improves scar detection; therefore, its clinical impact is unclear. Further evaluation in a large cohort of patients with nontransmural infarct is needed to further evaluate this sequence.

CONCLUSIONS

The DB-LGE sequence simultaneously nulls both normal myocardium and the blood-pool signal based on differences between their T_2 values. The proposed simple contrast-scout scan will replace the Look-Locker sequence to identify the timing parameter of DB-LGE, analogous to the Look-Locker inversion-time selection in standard LGE sequence.

ACKNOWLEDGMENTS

The phantom was graciously provided by Dr. James Moon and Gaby Capture. We thank Sophie Berg, RN, Kraig Kissinger, RT, and Beth Goddu, RT, for their help with patient recruitment and scanning of animals and patients. M.T. is a research fellow supported by the Sarnoff Cardiovascular Research Foundation, Great Falls, Virginia, USA.

REFERENCES

1. Raman SV, Simonetti OP, Winner MW, Dickerson Ja, He X, Mazzaferri EL, Ambrosio G. Cardiac magnetic resonance with edema imaging identifies myocardium at risk and predicts worse outcome in patients with non-ST-segment elevation acute coronary syndrome. J Am Coll Cardiol 2010;55:2480–2488.
2. Kwon DH, Asamoto L, Popovic ZB, Kusunose K, Robinson M, Desai M, Marwick TH, Flamm SD. Infarct characterization and quantification by delayed enhancement cardiac magnetic resonance imaging is a powerful independent and incremental predictor of mortality in patients with advanced ischemic cardiomyopathy. Circ Cardiovasc Imaging 2014;7:796–804.
3. Kwong RY, Chan AK, Brown KA, Chan CW, Reynolds HG, Tsang S, Davis RB. Impact of unrecognized myocardial scar detected by cardiac magnetic resonance imaging on event-free survival in patients presenting with signs or symptoms of coronary artery disease. Circulation 2006;113:2733–2743.
4. Rayatzadeh H, Tan A, Chan RH, et al. Scar heterogeneity on cardiovascular magnetic resonance as a predictor of appropriate implantable cardioverter defibrillator therapy. J Cardiovasc Magn Reson 2013;15:31.
5. O'Hanlon R, Grasso A, Roughton M, et al. Prognostic significance of myocardial fibrosis in hypertrophic cardiomyopathy. J Am Coll Cardiol 2010;56:867–874.
6. Chan RH, Maron BJ, Olivotto I, et al. Significance of late gadolinium enhancement at right ventricular attachment to ventricular septum in patients with hypertrophic cardiomyopathy. Am J Cardiol 2015;116:436–441.
7. Gulati A, Jabbour A, Ismail TF, et al. Association of fibrosis with mortality and sudden cardiac death in patients with nonischemic dilated cardiomyopathy. JAMA 2013;309:896–908.
8. Han Y, Peters DC, Salton CJ, Bzymek D, Nezafat R, Goddu B, Kissinger KV, Zimetbaum PJ, Manning WJ, Yeon SB. Cardiovascular magnetic resonance characterization of mitral valve prolapse. JACC Cardiovasc Imaging 2008;1:294–303.
9. Kellman P, Arai AE. Cardiac imaging techniques for physicians: late enhancement. J Magn Reson Imaging 2012;36:529–542.
10. Look DC, Locker DR. Time saving in measurement of NMR and EPR relaxation times. Rev Sci Instrum 1970;41:250–251.
11. Gupta A, Lee VS, Chung Y-c, Babb JS, Simonetti OP. Myocardial infarction: optimization of inversion times at delayed contrast-enhanced MR imaging. Radiology 2004;233:921–926.
12. Peters DC, Appelbaum EA, Nezafat R, Dokhan B, Han Y, Kissinger KV, Goddu B, Manning WJ. Left ventricular infarct size, peri-infarct zone, and papillary scar measurements: a comparison of high-resolution 3D and conventional 2D late gadolinium enhancement cardiac MR. J Magn Reson Imaging 2009;30:794–800.
13. Akçakaya M, Rayatzadeh H, Basha TA, Hong SN, Chan RH, Kissinger KV, Hauser TH, Josephson ME, Manning WJ, Nezafat R. Accelerated late gadolinium enhancement cardiac MR imaging with isotropic spatial resolution using compressed sensing: initial experience. Radiology 2012;264:691–699.
14. Kellman P, Arai AE, McVeigh ER, Aletras AH. Phase-sensitive inversion recovery for detecting myocardial infarction using gadolinium-delayed hyperenhancement. Magn Reson Med 2002;47:372–383.
15. Moghari MH, Peters DC, Smink J, Goepfert L, Kissinger KV, Goddu B, Hauser TH, Josephson ME, Manning WJ, Nezafat R. Pulmonary vein inflow artifact reduction for free-breathing left atrium late gadolinium enhancement. Magn Reson Med 2011;66:180–186.
16. Roujol S, Basha TA, Akçakaya M, Foppa M, Chan RH, Kissinger KV, Goddu B, Berg S, Manning WJ, Nezafat R. 3D late gadolinium enhancement in a single prolonged breath-hold using supplemental oxygenation and hyperventilation. Magn Reson Med 2013;857:850–857.
17. Daccarett M, McGann CJ, Akoum NW, MacLeod RS, Marrouche NF. MRI of the left atrium: predicting clinical outcomes in patients with atrial fibrillation. Expert Rev Cardiovasc Ther 2011;9:105–111.
18. Marrouche NF, Wilber D, Hindricks G, et al. Association of atrial tissue fibrosis identified by delayed enhancement MRI and atrial fibrillation catheter ablation: the DECAAF study. JAMA 2014;311:498–506.
19. Peters DC, Wylie JV, Hauser TH, Kissinger KV, Botnar RM, Essebag V, Josephson ME, Manning WJ. Detection of pulmonary vein and left atrial scar after catheter ablation with three-dimensional navigator-gated delayed enhancement MR imaging: initial experience. Radiology 2007;243:690–695.
20. Te Riele AS, Tandri H, Bluemke DA. Arrhythmogenic right ventricular cardiomyopathy (ARVC): cardiovascular magnetic resonance update. J Cardiovasc Magn Reson 2014;16:50.

21. Farrelly C, Rehwald W, Salerno M, Davarpanah A, Keeling AN, Jacobson JT, Carr JC. Improved detection of subendocardial hyperenhancement in myocardial infarction using dark blood–pool delayed enhancement MRI. Am J Roentgenol 2011;196:339–348.
22. Peel SA, Morton G, Chiribiri A, Schuster A, Nagel E, Botnar RM. Dual inversion-recovery MR imaging sequence for reduced blood signal on late gadolinium-enhanced images of myocardial scar. Radiology 2012;264:242–249.
23. Yarnykh VL, Yuan C. T1-insensitive flow suppression using quadruple inversion-recovery. Magn Reson Med 2002;48:899–905.
24. Kim HW, Rehwald WG, Wendell DC, Jenista ER, Assche LV, Jensen C, Filev P, Chen E-L, Parker Ma, Kim RJ. Black-blood contrast-enhanced MRI: validation of a novel technique for the diagnosis of myocardial infarction. In Proceedings of the 23rd Annual Meeting of ISMRM, Toronto, Ontario, Canada, 2015. p 662.
25. Koktzoglou I, Chung YC, Mani V, Carroll TJ, Morasch MD, Mizsei G, Simonetti OP, Fayad ZA, Li D. Multislice dark-blood carotid artery wall imaging: a 1.5 T and 3.0 T comparison. J Magn Reson Imaging 2006;23:699–705.
26. Nguyen TD, de Rochefort L, Spincemaille P, Cham MD, Weinsaft JW, Prince MR, Wang Y. Effective motion-sensitizing magnetization preparation for black blood magnetic resonance imaging of the heart. J Magn Reson Imaging 2008;28:1092–1100.
27. Srinivasan S, Hu P, Kissinger KV, Goddu B, Goepfert L, Schmidt EJ, Kozerke S, Nezafat R. Free-breathing 3D whole-heart black-blood imaging with motion sensitized driven equilibrium. J Magn Reson Imaging 2012;36:379–386.
28. Salerno M, Epstein F, Kramer C. MADE: a dark-blood delayed enhancement sequence to improve detection of subendocardial infarcts (motion attenuated delayed enhancement). In Proceedings of the 17th Annual Meeting of ISMRM, Honolulu, Hawaii, USA, 2009. p 3914.
29. Bandettini WP, Kellman P, Mancini C, Booker OJ, Vasu S, Leung SW, Wilson JR, Shanbhag SM, Chen MY, Arai AE. MultiContrast Delayed Enhancement (MCODE) improves detection of subendocardial myocardial infarction by late gadolinium enhancement cardiovascular magnetic resonance: a clinical validation study. J Cardiovasc Magn Reson 2012;14:83.
30. Foo TKF, Wolff SD, Gupta SN, Kraitchman DL. Enhanced viability imaging: improved contrast in myocardial delayed enhancement using dual inversion time subtraction. Magn Reson Med 2005;53:1484–1489.
31. Kellman P, Chung YC, Simonetti OP, McVeigh ER, Arai AE. Multicontrast delayed enhancement provides improved contrast between myocardial infarction and blood pool. J Magn Reson Imaging 2005; 22:605–613.
32. Liu CY, Wieben O, Brittain JH, Reeder SB. Improved delayed enhanced myocardial imaging with T2-Prep inversion recovery magnetization preparation. J Magn Reson Imaging 2008;28:1280–1286.
33. Jerosch-Herold M, Sheridan DC, Kushner JD, Nauman D, Burgess D, Dutton D, Alharethi R, Li D, Hershberger RE. Cardiac magnetic resonance imaging of myocardial contrast uptake and blood flow in patients affected with idiopathic or familial dilated cardiomyopathy. Am J Physiol Heart Circ Physiol 2008;295:H1234–H1242.
34. Kawel N, Nacif M, Santini F, Liu S, Bremerich J, Arai AE, Bluemke DA. Partition coefficients for gadolinium chelates in the normal myocardium: comparison of gadopentetate dimeglumine and gadobenate dimeglumine. J Magn Reson Imaging 2012;36:733–737.
35. Pintaske J, Martirosian P, Graf H, Erb G, Lodemann K-P, Claussen CD, Schick F. Relaxivity of gadopentetate dimeglumine (Magnevist), gadobutrol (Gadovist), and gadobenate dimeglumine (MultiHance) in human blood plasma at 0.2, 1.5, and 3 Tesla. Invest Radiol 2006;41: 213–221.
36. Spinazzi A, Lorusso V, Pirovano G, Kirchin M. Safety, tolerance, biodistribution, and MR imaging enhancement of the liver with gadobenate dimeglumine: results of clinical pharmacologic and pilot imaging studies in nonpatient and patient volunteers. Acad Radiol 1999;6:282–291.
37. Captur G, Gatehouse P, Keenan KE, et al. A medical device-grade T1 and ECV phantom for global T1 mapping quality assurance—the T1 mapping and ECV standardization in cardiovascular magnetic resonance (T1MES) program. J Cardiovasc Magn Reson 2016;18:58.
38. Moghari MH, Chan RH, Hong SN, Shaw JL, Goepfert LA, Kissinger KV, Goddu B, Josephson ME, Manning WJ, Nezafat R. Free-breathing cardiac MR with a fixed navigator efficiency using adaptive gating window size. Magn Reson Med 2012;68:1866–1875.
39. Tschabrunn CM, Roujol S, Nezafat R, Faulkner-Jones B, Buxton AE, Josephson ME, Anter E. A swine model of infarct-related reentrant ventricular tachycardia: electroanatomic, magnetic resonance, and histopathological characterization. Heart Rhythm 2015;13:262–273.
40. Pruessmann KP, Weiger M, Scheidegger MB, Boesiger P. SENSE: sensitivity encoding for fast MRI. Magn Reson Med 1999;42:952–962.
41. Bangerter NK, Cukur T, Hargreaves BA, Hu BS, Brittain JH, Park D, Gold GE, Nishimura DG. Three-dimensional fluid-suppressed T2-prep flow-independent peripheral angiography using balanced SSFP. Magn Reson Imaging 2011;29:1119–1124.
42. Kellman P, Olivieri L, Grant E, Berul CI, O'Brien K, Ratnayaka K, Hansen MS. Dark blood late gadolinium enhancement improves conspicuity of ablation lesions. J Cardiovasc Magn Reson 2016;18:1–2.
43. Tschabrunn CM, Roujol S, Nezafat R, Faulkner-Jones B, Buxton AE, Josephson ME, Anter E. A swine model of infarct-related reentrant ventricular tachycardia: electroanatomic, magnetic resonance, and histopathological characterization. Heart Rhythm 2016;13:262–273.

SUPPORTING INFORMATION

Additional Supporting Information may be found in the online version of this article.

Fig. S1. (**a**) Pulse sequence diagram of the proposed T_2 Prep-IR DB-LGE pulse sequence with an inversion pulse (INV) followed by a T_2 Prep pulse. The magnetization labels (M) correspond to Equations [a]–[d]. (**b**) Pulse sequence diagram of theoretical alternative T_2 Prep-IR pulse sequence; magnetization labels (M) correspond to Equations [i]–[iv].

Fig. S2. Simulations of the normalized magnetization of normal myocardium (green), blood (red), and scar (blue) at the beginning of each heart beat over 20 heart beat cycles. The simulations show that the magnetization reaches a steady state after the first cycle and do not change with scanning parameters (ie, Δt_1, Δt_2, Δt_3, flip angle (FA), and serum gadolinium concentration (Gd) are varied). The steady-state value does vary noticeably with heart rate (HR), but the steady state of all three tissues respond similarly to changes in the heart rate. Moreover, the change in the steady-state value is small for expected heart-rate variations over the course of a single scan ($<$ 10 bpm).

Fig. S3. Two-dimensional simulations of normal myocardium and blood-pool signals with superimposed linear approximations of the zero crossing points (Eqs. [5] and [6]), demonstrating that the zero crossing points are approximately linear when Δt_2 is fixed at 35 ms.

Fig. S4. Plots of the SNR of each vial as well as the CNRs and SNRs between the scar (T_1/T_2 = 290/41 ms) and normal myocardium (T_1/T_2 = 547/42 ms) or blood (T_1/T_2 = 454/188 ms) vials.

Fig. S5. Theoretical schematic of contrast-scout sequence protocol: Δt_1 and Δt_3 are sampled to extrapolate the common nulling point. The opaque squares represent images acquired with different timing. The points are linearly interpolated to approximate the zero lines (dotted lines); the intersection gives the optimal nulling parameters. Arrows point to examples of images acquired during a contrast scout sequence; within each set, there is one image in which just the normal myocardium is nulled and one image in which just the blood pool is nulled.

Fig. S6. (**a**) Two-dimensional simulation of T_2 Prep-IR sequence proposed by Liu et al, in which a T_2 Prep pulse (duration Δt_2) is immediately followed by an inversion pulse (inversion time TI). A common nulling point exists, but a practical means of identifying the common nulling point is lacking. (**b**) Two-dimensional simulation of T_2 Prep-IR sequence if a delay of Δt_1 is inserted between the T_2 Prep pulse (Δt_2 = 35 ms) and the inversion (inversion time Δt_3). (**c**) Plot of the inversion time needed to simultaneously null normal myocardium and blood using T_2 Prep-IR 32, assuming the ideal T_2 Prep time. This simulation demonstrates the rapid change in the common nulling point during the contrast washout period.

Video S1. Comparison of LGE (left) and DB-LGE (right) scans from a swine with induced left anterior descending artery infarction and left ventricular enhancement.

Video S2. Comparison of LGE (left) and DB-LGE (right) scans from a 48-year-old man with a history of left ventricular infarction and apical enhancement.